TASK QUARTERLY 7 No 4 (2003), 611–621

DYNAMIC MEASUREMENT AND SIMULATION OF BULK SOLIDS DURING SILO DISCHARGE

MICHAEL OSTENDORF[1], JÖRG SCHWEDES[1],
JENS UWE BÖHRNSEN[2] AND HEINZ ANTES[2]

[1] *Institute of Mechanical Process Engineering, Technical University of Braunschweig, Volkmaroder Str. 4/5, D-38104 Braunschweig, Germany*
{*m.ostendorf, j.schwedes*}*@tu-bs.de*

[2] *Institute of Applied Mechanics, Technical University of Braunschweig, Spielmannstraße 11, D-38106 Braunschweig, Germany*
{*j.boehrnsen, h.antes*}*@tu-bs.de*

(Received 3 July 2003)

Abstract: This paper deals with the experimental investigation and numerical simulation of silo discharge processes, including dynamic interactions between silo filling and elastic silo walls.

The experiments have taken place in a large model silo with a height of 3m and a rectangular base of 800 to 400mm. Optical measurement techniques have been applied to investigate the flow profile, while load cells on the silo walls have registered the stress' evolution, *e.g.* a stress peak (switch) move from the outlet to the transition of hopper and shaft.

The measured data have been compared with simulation results of the Institute of Applied Mechanics at the Technical University of Braunschweig. It has been possible because the numerical simulation examples have been chosen to be similar to the experimental test silo. The discharge process in the simulation is described by a system of nonlinear differential equations. Via the Finite Element Method (FEM) based on an Eulerian reference frame deformation rate, velocity field, porosity and stress distribution can be calculated without the need for re-meshing the FE grid.

Keywords: bulk solid, silo, load cells, FEM, hypoplasticity, viscosity

Nomenclature

Φ – hopper angle against the axis,
λ – horizontal load ratio,
φ_e – effective angle of internal friction,
φ_c – critical angle of internal friction,
φ_w – angle of wall friction,
d_{50} – mean particle diameter,
ϱ_b – bulk solid density.

1. Introduction

During silo discharge phenomena like silo quaking occur, causing problems which may affect the silo's structure and the environment. Up to now, many of these problems have not been understood completely because dynamic effects, such as time-dependent change of the flow profile while discharging bulk solids, often called "silo honking" or "silo quaking", have not been investigated well enough.

Many authors have reported the occurrence of dynamic effects while discharging silos, among others, Levinson and Munch-Anderen [1] and Tejchman [2]. Tejchman has described discharging experiments with a cylindrical silo made of perspex. He has observed "strong vibrations", minimised using a rifled wall.

Measurements of flow patterns using optical flow analysis are common practice, *e.g.* see Schwedes [3] and Johanson [4]. In the former, the flow pattern was recorded by a conventional camera. More recent investigations of velocity profiles are accomplished using a CCD- or video-camera (*e.g.* Carson *et al.* [5]). Velocities are evaluated with a computer, whereby mean velocity with respect to time is calculated. Lueptow *et al.* [6] use Particle Image Velocimetry to analyse velocity profiles. In [7] a detailed description of how to use Particle Image Velocimetry with granular flows can be found.

For simulations of bulk solid flow, hypoplastic constitutive relations are used. The development of these models started from the hypoelastic theories of Truesdell [8] in 1955. In the research group of Gudehus [9] a comprehensive hypoplastic model for bulk solids has been developed wherein the fundamental hypoplastic constitutive equation was created by Kolymbas [10]. Bauer [11] and von Wolffersdorff [12] improved the hypoplastic formulation with density dependent behaviour including the void ratio and introduced material constants with more physical meaning.

2. Experimental setup

The stresses have been measured in a silo made of plane perspex walls and a steel framework as its support structure (Figure 1). For a constant discharge rate, a conveyor belt is placed below the orifice of the silo. Since the velocity of the conveyor belt is adjustable, the discharge rate can be changed up to 2kg/s. Special load cells (described by Schulze and Lyle [13]), mounted on the wall, measure normal forces and two perpendicular shear forces. Up to 8 of these cells can be used for one measurement (left side: L1 … L8, right side: R1 … R8). The deformation of the walls in the shaft region can be measured with 4 strain gauges (W1 … W4). The whole structure rests on 3 load cells (B1 … B3). Thus, the amount of bulk solids in the silo is known. All data are collected with a PC with a scan rate of 5.000 data points per seconds.

Additionally to the stress measurements, bulk solids are observed optically with a CCD-Camera; the velocities of the bulk solids are determined using Particle Image Velocimetry (see Lueptow *et al.* [6] and Ostendorf *et al.* [7]).

Three different bulk solids: PET ($\varphi_e = 30^\circ \quad \varphi_c = 44^\circ$), PP ($\varphi_e = 29^\circ \quad \varphi_c = 39^\circ$) and PS ($\varphi_e = 29^\circ \quad \varphi_c = 42^\circ$) have been used for the discharge experiments.

3. Numerical model

The Eulerian coordinate frame has been used for the description of granular flow. Thus, one can simulate discharge periods over a couple of seconds with no need

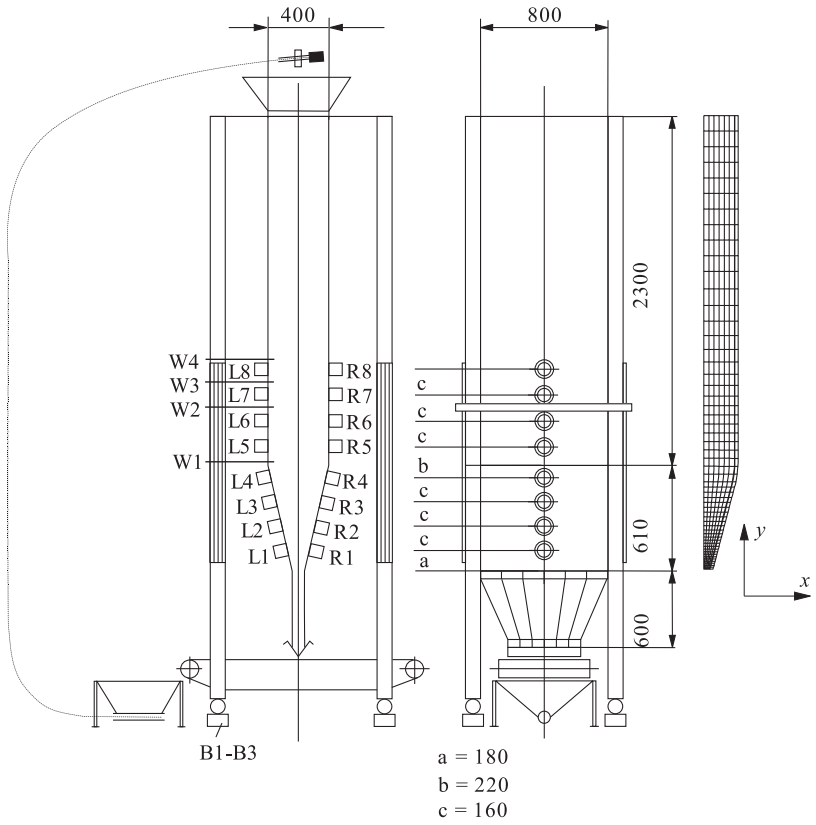

Figure 1. Experimental setup and FE grid: positions of load cells and strain gauges for the measurement of the stresses, wall deformations and silo mass; the FE grid represents a symmetric part of the silo

for re-meshing the finite element grid, since the coordinate frame is not moving, and, hence, the relative velocity $\mathbf{c}$ becomes equal to the material velocity $\mathbf{v}$. The following differential equations hold for the Cauchy stress tensor $\mathbf{T}$, the density $\rho(\mathbf{x},t)$ of bulk solids, material velocity, $\mathbf{v}$, and the volume force $\mathbf{b}_v$ due to gravity:

- equation of momentum

$$\nabla\cdot\mathbf{T}+\rho(\mathbf{x},t)(\mathbf{b}_\mathbf{v}-\dot{\mathbf{v}})=\frac{\partial T_{ij}}{\partial x_i}+\rho(b_j-\frac{dv_j}{dt})=0; \tag{1}$$

- conservation of mass

$$\frac{\partial\rho}{\partial t}+\nabla\cdot(\rho\mathbf{v})=\frac{\partial\rho}{\partial t}+\rho\frac{\partial v_i}{\partial x_i}=0. \tag{2}$$

3.1. Hypoplastic model

Hypoplasticity describes inelastic phenomena without using additional terms like yield surface or plastic potential. It will not distinguish elastic deformations from plastic ones, *i.e.* inelastic deformations are recognised to affect the loading process from the beginning, and one uses a unique equation which combines stress, strain and material constants. A comprehensive introduction to hypoplasticity is given by Kolymbas [10].

The following definition of the Jaumann tensor $\mathbf{T}$ was introduced by Gudehus and v. Wolffersdorff 1996:

$$\mathbf{T} = f_b f_e \frac{1}{\mathrm{tr}(\hat{\mathbf{T}} \cdot \hat{\mathbf{T}})} \left[F^2 \mathbf{D} + a^2 \hat{\mathbf{T}} \, \mathrm{tr}(\hat{\mathbf{T}} \cdot \mathbf{D}) + f_d a F (\hat{\mathbf{T}} + \hat{\mathbf{T}}') \|\mathbf{D}\| \right] = \mathcal{H} : \mathbf{D}, \tag{3}$$

where $\mathbf{D} = \frac{1}{2}(\mathbf{v}\nabla + \nabla\mathbf{v})$ means the deformation rate, *i.e.* the symmetric part of the velocity gradient; $\mathbf{L} = \mathrm{grad}\mathbf{v}$; $\hat{\mathbf{T}} = \mathbf{T}/\mathrm{tr}\,\mathbf{T}$ and $\hat{\mathbf{T}}' = \hat{\mathbf{T}} - \frac{1}{3}\mathrm{tr}(\mathbf{T})\mathbf{I}$ are the so-called stress ratio tensor and its deviator, respectively. The barotropy factor, f_b, and the pycnotropy factors f_e and f_d depend on the void ratio $e = V/\Sigma \frac{m_{s_i}}{\rho_{s_i}} - 1$. The void ratio at isotropic compression, e_i, the void ratio at maximum compaction, e_d, and the void ratio at critical state, e_c (see Figure 2) are determined with shake tests. Granular stiffness, h_s, is determined with compaction tests and depends on hydrostatic pressure, $p_s = \mathrm{tr}(\mathbf{T})$. For a detailed description of the model parameters, see Herle [14] and Böhrnsen [15].

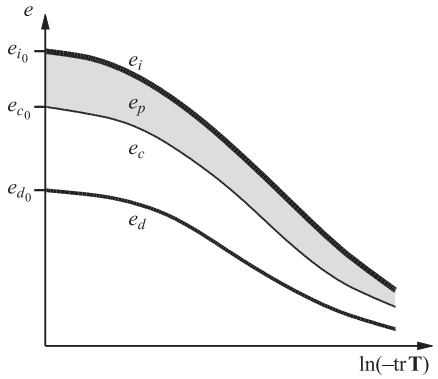

Figure 2. Void ratio, dependence on volumetric (hydrostatic) stress; e_i – upper limit, e_d – lower limit, e_c – critical void ratio and e_p – the SOM region (swept out of memory)

3.2. Viscosity

The viscous behaviour of bulk solids shear flow is known since Bagnold [16] 1954 and Savage [17] 1984. Hutter and Hwang have shown in [18] 1994 that the velocity-dependent behaviour of the general constitutive stress deviator can be derived from a rate-dependent functional, where the dynamic extension is represented by an additional term which includes the deformation tensor coupled with a viscous parameter. Thus, Equation (3) can be written in the following form by splitting $\mathbf{T}$ in to a static part $\mathbf{T}_s$ and a dynamic part $\mathbf{T}_v$:

$$\mathbf{T} = h(\mathbf{T},\mathbf{D}) + g(\mathbf{T},\mathbf{D},\mathbf{D}) = \mathbf{T}_s + \mathbf{T}_v = \mathcal{H} : \mathbf{D} + \mathcal{G} : \mathbf{D}. \tag{4}$$

The velocity-depended dynamic material tensor, $\mathcal{G}_{ijkl} \hat{=} 2\mu^* \sqrt{\mathrm{tr}\mathbf{D}'^2} \cdot (\delta_{ik}\delta_{jl}) = \gamma_{dyn} \cdot (\delta_{ik}\delta_{jl})$, is a description of a non-Newtonian fluid (formulated by Gladen [19]). The density-dependent viscous parameter $\mu^* = \left(\frac{\rho(t)}{\rho_0}\right)^{\psi} \cdot \mu_0^* [\mathrm{Ns/m^2}]$ is introduced here. ρ_0 means the bulk solid's density in the filling state, the parameter μ_0 and the exponent ψ are calibrated with experimental data. With a decrease of density during discharge, near the orifice, a decrease of viscosity takes place.

The dynamic material coefficient, $\gamma_{dyn} = 2\mu^* \sqrt{\mathrm{tr}\mathbf{D}'^2}\,[\mathrm{N/m^2}]$, describes the influence of shear deformation on viscous damping: with an increase of the deviatoric stretching rate, $\mathbf{D}'$, the influence of the viscous term increases.

3.3. Methodology of numerical solution

For solving the system of differential equations, the Finite Element Method is used (see [20]), where the variation of velocity, $\delta\mathbf{v}$, is taken as a weighing function. An implicit Euler integration schema is applied.

The calculation of the stress rate, $\mathbf{T}$, requires small time steps of 10^{-6}s. The hypoplastic formulation ensures a physically valid stress state, see [14].

For a 2D simulation of bulk solids and the wall, isoparametric 8-node elements are used with a 9-Gauss point integration for bulk solid elements and a 16-Gauss point integration for wall elements. The coupling between bulk elements and wall elements is realized by a special 6-node contact element with the assumption of Coulomb's law of friction.

Table 1 presents the material parameters used in the simulation. At the orifice a maximum outflow velocity of $v_y = 1\,\mathrm{cm/s}$ is prescribed as a kinematic boundary condition, *i.e.* starting from zero, the maximum velocity is reached after an opening period of 0.2sec.

Table 1. Material parameters used in the simulation: d_{50} – median diameter, ρ_b – bulk density, φ_c – internal friction, φ_w – wall friction, λ – pressure ratio

Bulk solids	d_{50}	ρ_b	φ_c	φ_w	λ
PET pellets	3.05mm	950kg/m^3	28°	15°	0.41

4. Results

4.1. Flow profile

In Figure 3, the numerically simulated velocity field is compared with the results of the experiment. The simulation gives velocities at each point of the FE grid. In the experiment the video data obtained from the CCD camera is applied with Particle Image Velocimetry (PIV). The measured velocities are time-averaged over 4sec.

The simulated velocity profile and the experimentally determined velocities in the hopper region are shown in Figure 3; good agreement between simulation and experiment can be seen. The velocities at the outlet are approximately the same due to the fact that the boundary condition of the simulation uses the given velocity of the conveyor belt. The measured velocities in the upper region are slightly smaller than the calculated ones.

Having a closer look at the velocities, it can be seen that the simulated directions of vectors near the outlet are along the hopper walls, while the experimental velocities are not. Further, the velocities near the wall at the outlet are smaller in the experiments than in the simulation. The probable reason is that the viscosity parameter in the simulation is too small. The viscosity results from shear tests, which are difficult to perform for coarse bulk solids.

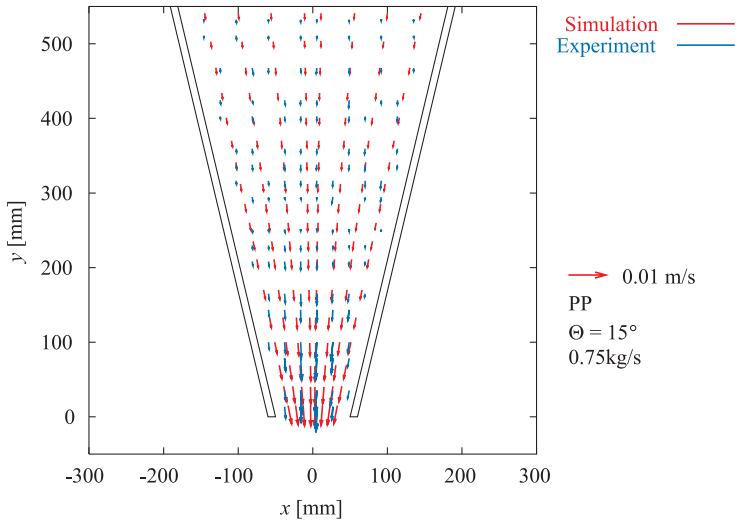

Figure 3. Comparison of simulation and experiment: velocity profile in the hopper during discharge

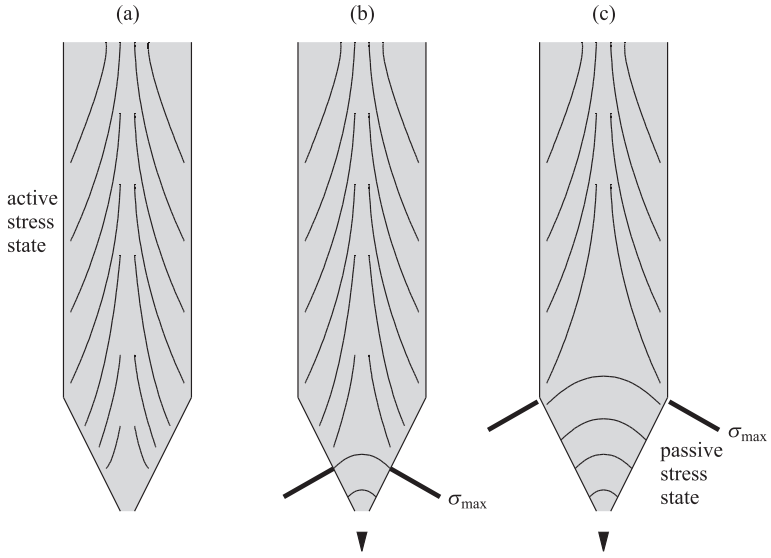

Figure 4. Principle stress trajectories and maximum normal wall stress: change from the active to the passive stress state in the hopper and upward movement of the stress peak at the beginning of discharge

4.2. Stress distribution

4.2.1. Beginning of discharge

At the beginning of discharge, the stress state of the bulk solid in the hopper changes from the filling state, where the major principal stress is vertical at the axis, to the discharge state, where major principal stress is horizontal at the axis. The change starts from the bottom of the silo, moving upwards to the transition of the hopper and the shaft. This change of stress state is called a "switch". In Figure 4 the mechanism of a moving switch is illustrated. The filling state of a bulk solid in the

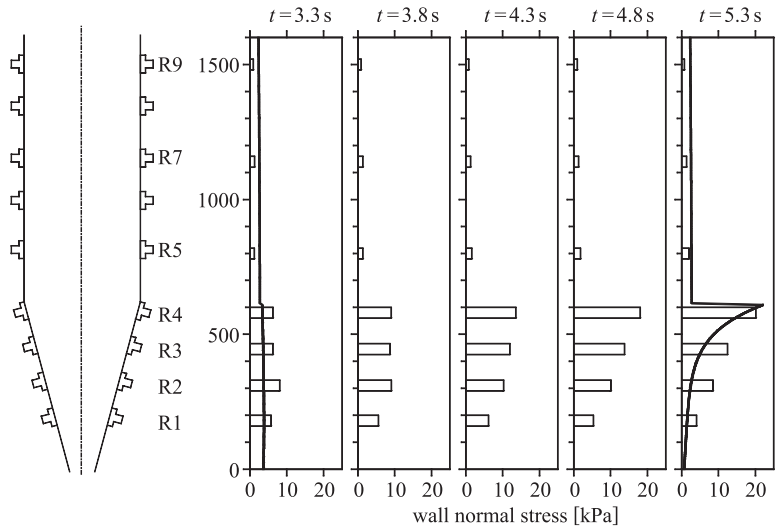

Figure 5. Wall normal stress in the experimental silo at various time steps: measured results at load cell positions R (bars) and analytical results of the filling state and the discharge state (lines) [21]

hopper is shown in Figure 4a for the ideal case. In this case, the stress state is called an "active stress state".

At the transition of the stress state a peak of the wall's normal stress occurs. The increase of wall stress is due to the fact that on the onset of flow the lowest layer dilates first, whereas the layers above are not moving yet. Due to dilation, the bulk solid's density, strength and, hence, supporting stresses are decreasing for the layers above (Figure 4b). As a result, normal and shear stresses on the wall must increase to fulfill the equilibrium of forces in the layer above. The dilation front moves upwards; the change of the stress state and, therefore, the switch are moving upwards from the orifice and rest at the transition of the hopper and the shaft, as the stress state in the shaft of the silo remains active (Figure 4b and 4c).

In Figure 5 stress profiles at five different points of time measured in the test silo are shown. The material used was PET. Until a time of $t = 3$s the silo was in the filling state, because the start of discharge is delayed after the starting of the measurements. At a point of time of $t = 5.3$s the discharge state in the silo was fully developed. In the first and last diagram ($t = 3.3$s and $t = 5.3$s, respectively) theoretical values for the filling and discharge states are displayed as lines. The values were calculated with the "stresstool" program published by Schulze [21]. The program calculates the stresses for the shaft according to the theory of Janssen [22]. In the hopper region, the program distinguishes between the filling and the discharge states. The filling state is calculated according to Motzkus, while the discharge state is calculated according to the proposal of Arnold and McLean, where the theory of Jenike is applied. It can be seen that the stresses measured in the hopper are higher than the theoretical values, whereas in the shaft the measured stresses are less then the calculated values. One possible reason for this result may be that the way of filling the silo did not lead to an active stress state. Another reason could be that the bulk solid's properties were not measured precisely. In the case of the material used it is possible, as the particle size

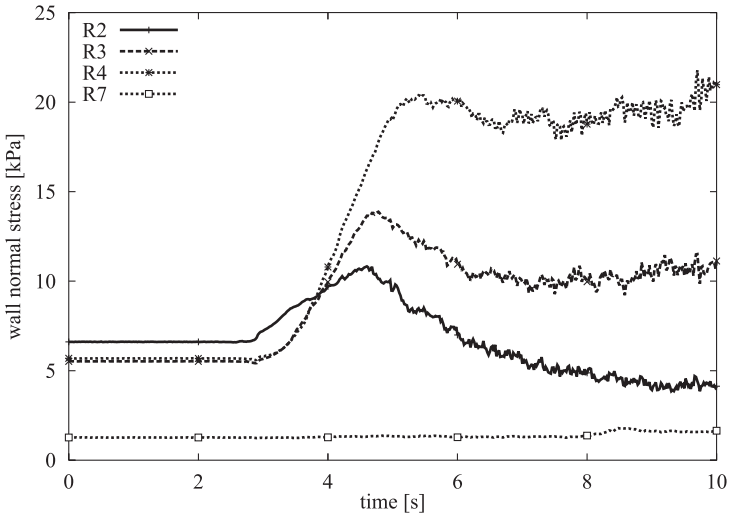

Figure 6. Experiment: wall normal stress at various load cell positions, R, in the hopper and the shaft

is large. With bulk solids of large particle sizes an exact determination of properties is difficult. Nevertheless, maximal stresses near the transition of the hopper and the shaft are the same in the theory and in the experiment.

The three middle diagrams show how the discharge state develops from the filling state. The stresses in the hopper all increase first, after the beginning of discharge, and then decrease, first at the bottom of the hopper, later in the higher regions of the hopper. This behaviour is due to the change of the stress state from an active stress state after filling to a passive stress state after the beginning of discharge, described before as the "switch". At the transition of the hopper and the shaft the switch comes to rest; there is no recognizable change of the stress state in the shaft. It cannot be seen clearly in Figure 5 that the stress peak caused by the switch moves upwards in the hopper.

Nevertheless, the switch is moving up the hopper from the outlet towards the transition from the hopper to the shaft. This can be seen more clearly in Figure 6. In this diagram the stresses of the load cells R2, R3, R4 (the hopper) and R7 (the shaft) are shown versus time for the same experiment as in Figure 5 (for positions see Figure 1). For each load cell in the hopper a stress peak can be determined. At this point of time the stress state changes from the active to the passive stress state. The higher the load cell is situated in the hopper, the later the stress peak occurs. In the shaft, no substantial change in the stress state can be determined.

In Figure 7 results of the simulations are shown. The simulated rate of deformation, $\mathbf{D}$, normal to the silo walls at various heights is shown versus time. The rate of deformation, $\mathbf{D}$, is calculated directly by the FEM. A negative deformation rate leads to an increase in the stresses. The simulated positions are similar to those of the load cells shown in Figure 6.

It can be seen that the switch occurs in the hopper and moves upwards, characterised by a decrease of $\mathbf{D}$ with a resulting stress increase. In the shaft, the stress decreases slightly, as indicated by an increase of the deformation rate (unloading).

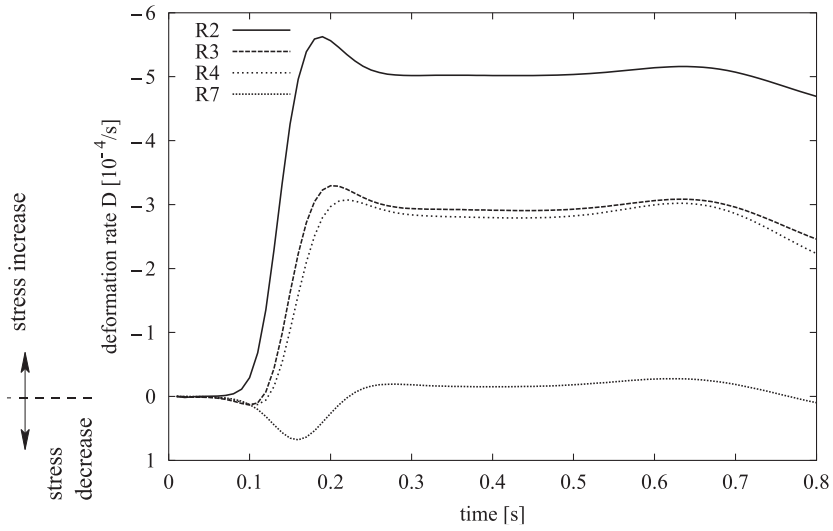

Figure 7. Simulation: wall normal rate of deformation at various load cell positions, R, in the hopper and the shaft

This is because the density and, thus, also the strength of the bulk solid in the shaft decreases near the transition. This behaviour of bulk solids can also be seen in the experiments, but because of the scaling it is not apparent in Figure 6.

4.2.2. Fluctuations during discharge

When the discharge state is reached, the flow of the bulk solid is called a "steady state flow" because the stresses and the bulk solid's density do not change any more. This statement is valid for time averaged data. When looking at the instantaneous flow, the situation is different. In Figure 8, a closer view of the stresses at the transition of the hopper and the shaft is given for the wall normal stress near the transition at the L4 and R4 positions (see Figure 1).

It can be seen that, although the discharge state has been reached, the stresses at the transition are not constant but alternating on the left and right sides of the silo. A frequency with a time period of approximately 5 seconds has been determined for these fluctuations. The discharge rate for this measurement is about 5kg/s; similar results were published by Hardow [23].

For other angles and discharge rates the determined frequency is different. In Figure 9 the obtained frequency is plotted versus the discharge rate for PET pellets in two silos with different hopper angles. It can be seen that the frequency increases linearly with the discharge rate.

Most probably, moving shear bands are responsible for this effect. The occurrence of shear bands has been described by Blair-Fish and Bransby [24]. The simulation cannot describe an alternating state because of the applied symmetric approach and uniform filling. Furthermore, the FE method with its continuum mechanical approach is not yet able to consider moving shear bands. If shear bands are the reason for these fluctations' then, as per Figure 9, it can be concluded that the amount of bulk solid between two shear bands is constant. This means that the developement of

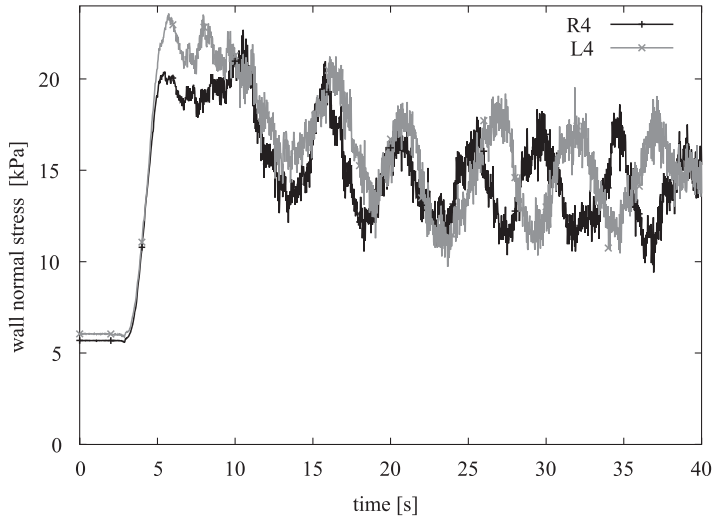

Figure 8. Measured stress distribution: alternating stress fluctuation in the hopper

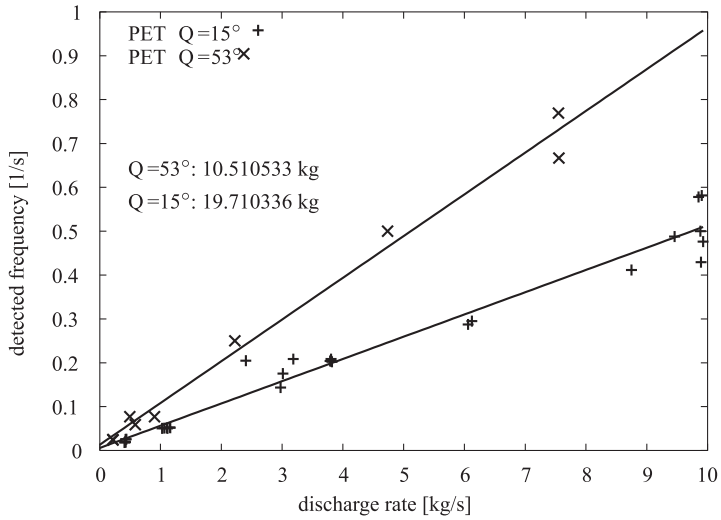

Figure 9. Dependence of stress fluctuation on the discharge rate and the hopper angle

shear zone does not depend on the discharge rate in the region from 0.3 up to 10 kg/s for PET pellets.

Further investigations have shown that the development of shear bands also depends on the material used. The fluctuations of polypropylene (PP) and polystyrol (PS) pellets are not as regular as these shown for PET pellets. The reason for this might be seen in the different shapes and hardness of the pellets.

5. Conclusion

Stress measurements in a large-scale silo with various bulk solids have shown that at the beginning of discharge the "switch" is moving upwards, from the bottom to the transition from the hopper to the shaft. Using a hypoplastic model improved with a density-dependent viscosity formulation, the simulation is a convergent and rather

effective approach to simulation of bulk-solid silo discharge. The moving switch can be detected (Figure 7) and the velocity distribution (Figure 3) shows a satisfactory agreement with the experimental data.

After the beginning of discharge fluctuations beneath the transition of the hopper and the shaft occur. The peaks of these fluctuations first develop at the same time right and left. After a short time, though, the peaks alternate. The amount of bulk solid being discharged between two peaks does not depend on the discharge rate but rather on the geometry of the silo and the bulk solid material.

It is planned to perform velocity measurements at the same time using the PIV method for stress measurements. Thus, we will be able correlate the velocity and stress fluctuations to better understand the observed dynamic effects.

References

[1] Levinson B and Munch-Andersen J 1994 *Powder handling and processing* **6** 385

[2] Tejchman J 1997 *Modelling of Shear Localication and Autogeneous Dynamic Effects in Granular Bodies*, Habilitation, Institut für Boden- und Felsmechanik, Karlsruhe

[3] Schwedes J 1968 *Fließverhalten von Schüttgütern in Bunkern*, Verlag, Chemie, Weinheim

[4] Johanson J 1964 *Int. J. Appl. Mech.* **31** 499

[5] Khelil A, Weisse D and Roth J C 1989 *Powders and Grains*, Balkema, Rotterdam, pp. 461–468

[6] Lueptow R, Akonur A and Shinbrt T 2000 *Exp. Fluids* **28** (21) 183

[7] Ostendorf M and Schwedes J 2001 *Handbook of Powder Technology* (Levi A and Kalman H, Eds), Elsevier, pp. 851–860

[8] Truesdell C 1955 *J. Rational Mech. Anal.* **4** 83

[9] Gudehus G 1996 *Soils and Foundations* **36** (1) 1

[10] Kolymbas D 2000 *Introduction to Hypoplasticity* (Balkema A A, Ed.), Rotterdam, Netherlands

[11] Bauer E 1996 *Soils and Foundations* **36** (1) 13

[12] von Wolffersdorff P A 1996 *Mechanics of Cohesive-Frictional Materials* **1** 251

[13] Schulze D and Lyle C 1989 *Reports in Applied Measurements* **4** 34

[14] Herle I 1997 *Hypoplastizität und Granulometrie einfacher Korngerüste*, PhD Thesis, Institut für Boden- und Felsmechanik, Karlsruhe

[15] Böhrnsen J U 2002 *Braunschweiger Schriften zur Mechanik* **45** 29

[16] Bagnold R A 1954 *Proc. Royal Society*, London, **A 225** pp. 49–63

[17] Savage S B and Sayed M 1984 *J. Fluid Mech.* **142** 391

[18] Hwang H 1994 *Ein neues kinetisches Modell für rasche Granulatströmung*, PhD Thesis, Fachbereich Mechanik, Technische Hochschule, Darmstadt

[19] Gladen W 1985 *Numerische Untersuchung der Lasten in Silozellen beim exzentrischen Entleeren*, PhD Thesis, Institut für Boden- und Felsmechanik, Karlsruhe

[20] Böhrnsen J U and Antes H 2000 *3rd Israeli Conf. Conveying and Handling of Particulate Solids* (Kalman M H H and Levy A, Eds) **I** pp. 4.18–4.24

[21] Schulze D 2001 *Silo Stress Tool*, http://members.aol.com/SchulzeWF/sstzip.exe

[22] Janssen H 1895 *VDI-Zeitschrift* **39** (35) 1045

[23] Hardow B 1999 *Spannungsschwankungen im Schüttgut beim Entleeren aus einem Silo*, PhD Thesis, TU-Braunschweig

[24] Blair-Fish P M and Bransby P L 1973 *J. Eng. Ind. Trans. ASME* **B 95** (1) 17